CHEMISTRY OF MATERIALS

ARTICLE

pubs.acs.org/cm

Structural Isomerism and Effect of Fluorination on Gas Adsorption in Copper-Tetrazolate Based Metal Organic Frameworks

Pradip Pachfule,[†] Yifei Chen,[‡] Subash Chandra Sahoo,[†] Jianwen Jiang,[‡] and Rahul Banerjee*[,†]

[†]Physical/Materials Chemistry Division, National Chemical Laboratory, Dr. Homi Bhabha Road, Pune, Maharashtra 411008, India

[‡]Department of Chemical and Biomolecular Engineering, National University of Singapore, 117576 Singapore

Supporting Information

ABSTRACT: Synthesis, structure, and gas adsorption properties of three Metal Organic Frameworks (MOFs) synthesized from predesigned ligands 4-(1*H*-tetrazole-5-yl)benzoic acid (**4-TBA**) and 2-fluoro-4-(1*H*-tetrazole-5-yl)benzoic acid (**2F-4-TBA**) along with Cu(II) as an metal precursor has been reported. Among these MOFs, $Cu_9(4\text{-TBA})_{10}(C_2H_5OH)_2$ (**Cu-TBA-1**) and $Cu_2(4\text{-TBA})_2(DMF)(C_2H_5OH)$ (**Cu-TBA-2**) are structural isomers. Whereas, $Cu_2(4\text{-TBA})_2(DMF)(C_2H_5OH)$ (**Cu-TBA-2**) and $Cu_2(2\text{-F-4-TBA})_2(DMF)_2$ (**Cu-TBA-2F**) have similar crystal structure. N_2 adsorption isotherms of the activated sample of Cu-TBA-1 and -2 exhibit types-I sorption behavior with a Langmuir and Brunauer−Emmett−Teller (BET) surface area of 686, 402 m^2/g and 616, 356 m^2/g, respectively. It is noteworthy that Cu-TBA-1 and -2 adsorbs 1.16 and, 1.54 wt % H_2, while Cu-TBA-2F adsorbs 0.67 wt % at 77 K and 1 atm. On the other hand, Cu-TBA-1 and -2 adsorb 3.08 and 2.54 mmol/g, while Cu-TBA-2F adsorbs 1.27 mmol/g of CO_2 at 298 K and 1 bar pressure. H_2 adsorption sites in Cu-TBA-2 and -2F have been analyzed by molecular simulation.

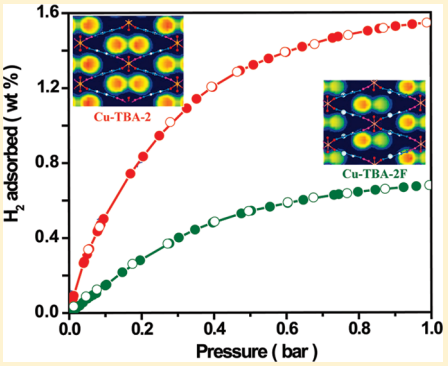

KEYWORDS: metal−organic framework, structural isomerism, fluorination, hydrogen storage, CO_2 adsorption

INTRODUCTION

Recent years have witnessed a huge level of research on the synthesis of porous functional materials named Metal Organic Frameworks (MOFs), using diverse organic spacers with different metals.[1] One of the major reasons for MOF research is the expectation of achieving the U.S. Department of Energy (DoE) targets on H_2 storage for on-board and vehicular applications.[2] It is noteworthy that, active research for storing hydrogen is also ongoing on functionalized and nonfunctionalized carbon nanotubes,[3] zeolites,[4] activated carbon,[5] and metal hydrides.[6] Although these materials have been extensively studied and potentially applied in several ways, still there are limitations for using these materials as they are expensive, shows strong interaction with adsorbents, problems in regeneration of adsorbents, and so forth. MOFs on the other hand have shown promise over these materials because of their fascinating structures, exceptionally high surface areas, uniform yet tunable pore sizes, and well-defined adsorbate-MOF interaction sites.[7] Various strategies such as extending pore sizes comparable to the adsorbed molecules,[8] increasing surface area and pore volume,[9] utilizing catenation,[10] and creation of open metal sites[11] have been explored, to achieve the DoE target for H_2 storage. Similarly, insertion of functionalized links like −F, $-NH_2$, −OH, −COOH, and so forth on the organic spacer has also been proven to have a good impact on enhancing the H_2 and CO_2 gas adsorption properties.[12] Recently, computational studies proved that the choice of both ligand and metal center plays an important role in gas-framework interactions.[13] In their recent report, Yang et al. and Cheetham and co-workers have showed that porous MOFs with exposed fluorine atoms (F-MOFs), show "*high*" physisorptive hydrogen adsorption enthalpy resulting in the enhancement of the H_2 adsorption properties.[14] However, in another work on partially fluorinated MOFs, Kim et al. had made explicit comparison with nonfluorinated analogues and imparted a "*disadvantage*" for fluorination toward H_2 adsorption.[15] As a result, it is very difficult to draw any conclusion regarding the impact of fluorination on H_2 and CO_2 adsorption as there are very few systematic comparative studies of gas storage in iso-structural fluorinated and nonfluorinated MOFs.

Herein, we represent the synthesis, structure, and gas adsorption properties of three MOFs[16] synthesized from predesigned ligands 4-(1*H*-tetrazole-5-yl)benzoic acid (**4-TBA**)[17] and 2-fluoro-4-(1*H*-tetrazole-5-yl)benzoic acid (**2F-4-TBA**)[17] with Cu(II) as an metal precursor. Among these MOFs, $Cu_9(4\text{-TBA})_{10}(C_2H_5OH)_2$ (**Cu-TBA-1**) and $Cu_2(4\text{-TBA})_2(DMF)(C_2H_5OH)$ (**Cu-TBA-2**) are structural isomers. Whereas nonfluorinated $Cu_2(4\text{-TBA})_2(DMF)(C_2H_5OH)$ (**Cu-TBA-2**) and fluorinated $Cu_2(2\text{-F-4-TBA})_2(DMF)_2$ (**Cu-TBA-2F**) have similar crystal structure. These MOFs are characterized by single crystal X-ray diffraction. H_2 adsorption sites in Cu-TBA-2 and -2F have been analyzed computationally by a molecular simulation method. To the best of our knowledge this is the first report where the

Received: February 11, 2011
Revised: May 4, 2011
Published: May 17, 2011

effect of fluorination on structurally similar MOFs has been verified both experimentally and computationally.

EXPERIMENTAL SECTION

All reagents and solvents for synthesis and analysis were commercially available and used as received. The Fourier transform (FT) IR spectra were taken on a Bruker Optics ALPHA-E spectrometer with a universal Zn−Se ATR accessory in the 600−4000 cm^{-1} region. Powder X-ray diffraction (PXRD) patterns and in situ variable temperature PXRD (VT-PXRD) were recorded on a Phillips PANalytical diffractometer for Cu K_α radiation (λ = 1.5406 Å), with a scan speed of 2° min^{-1} and a step size of 0.02° in 2θ. Thermo-gravimetric analysis (TGA) experiments were carried out in the temperature range of 20−800 °C on a SDT Q600 TG-DTA analyzer under N_2 atmosphere at a heating rate of 10 °C min^{-1}. All low pressure gas adsorption experiments (up to 1 bar) were performed on a Quantachrome Quadrasorb automatic volumetric instrument. The ligands used for the synthesis of all MOFs reported in this paper were synthesized and purified by the previously reported procedure.[18]

Cu_9(4-TBA)$_{10}$(C_2H_5OH)$_2$ (Cu-TBA-1). A 2.0 mL portion of 4-TBA solution (0.20 M) in 1:1 solution of *N*,*N*-dimethylformamide (DMF) and ethanol (EtOH) was taken in a 5 mL vial. A 0.5 mL portion of $Cu(NO_3)_2 \cdot 3H_2O$ solution (0.20 M) in DMF was added to this solution. The vial was capped and heated to 85 °C for 96 h. The mother liquor was decanted, and the octahedral blue crystals were filtered off and washed with EtOH. The unreacted ligand can be removed by washing in DMF (3 mL, 4 times) as 4-TBA is highly soluble in DMF, and afterward the resulting MOF was dried in air (10 min). [**Yield:** 54%, 0.0130 g depending on $Cu(NO_3)_2 \cdot 3H_2O$]. ***FT-IR:*** (KBr 4000−600 cm^{-1}): 3039(m, br), 2795(w, br), 2356(m), 1660(s), 1611(s), 1393(s), 1246(m), 1091(s), 868(m), 742(m) cm^{-1}. **Element analysis:** Found (%) *C* = 39.20, *H* = 1.99, *N* = 22.24; Calc. (%) *C* = 40.24, *H* = 1.96, *N* = 21.82.

Cu_2(4-TBA)$_2$(DMF)(C_2H_5OH) (Cu-TBA-2). A 2.0 mL portion of 4-TBA solution (0.20 M) in 1:1 solution of DMF and EtOH was taken in a 5 mL vial. A 0.009 g portion (0.2 mmol) of anhydrous CuCl solid was added to this solution. Additional 0.5 mL of DMF was added to the above mixture; the vial was capped and heated at 90 °C for 72 h. After cooling to room temperature, two layers were seen, one was a plate light blue crystal of Cu-TBA-2 and other one was unreacted white starting materials. Then collected Cu-TBA-2 crystals were washed with EtOH (2 mL, 3 times) and DMF (5 mL, 2 times) and dried in air (10 min). [**Yield:** 61%, 0.0054 g depending on CuCl]. ***FT-IR:*** (KBr 4000−600 cm^{-1}): 3555(m, br), 2811(m), 2675(w), 2361(w), 1668(s), 1614(m), 1537(w), 1401(s), 1325(m), 1098(s), 860(m), 739(s) cm^{-1}. **Element analysis:** Found (%) *C* = 39.84, *H* = 3.59, *N* = 20.96; Calc. (%) *C* = 40.38, *H* = 3.71, *N* = 20.18.

Cu_2(2-F-4-TBA)$_2$(DMF)$_2$ (Cu-TBA-2F).[31] A 2.0 mL portion of 2-F-4-TBA solution (0.20 M) in 1:1 solution of DMF and EtOH was taken in a 5 mL vial. A 0.5 mL portion of $Cu(NO_3)_2 \cdot 3H_2O$ solution (0.20 M) in DMF was added to this solution. The vial was capped and heated to 85 °C for 96 h. The mother liquor was decanted, and plate like blue crystals were filtered off, washed with EtOH and dried in air (10 min). [**Yield:** 58%, 0.0139 g depending on $Cu(NO_3)_2 \cdot 3H_2O$]. ***FT-IR:*** (KBr 4000−600 cm^{-1}): 3561(m, br), 2923(m), 2853(w), 2458(w), 1745(s), 1537(s), 1380(s), 1212(s), 1090(m), 1020(s), 895(m), 752(s) cm^{-1}. **Element analysis:** Found (%) *C* = 40.02, *H* = 2.31, *N* = 21.84; Calc. (%) *C* = 40.61, *H* = 2.44, *N* = 21.21.

Single Crystal X-ray Diffraction. All single crystal data were collected on a Bruker *SMART APEX* three circle diffractometer equipped with a *CCD* area detector (Bruker Systems Inc., 1999a)[19] and operated at 1500 W power (50 kV, 30 mA) to generate Mo K_α radiation (λ = 0.71073 Å). The incident X-ray beam was focused and monochromated using Bruker Excalibur Gobel mirror optics. Crystals of the MOFs reported in the paper were mounted on nylon CryoLoops (Hampton Research) with Paraton-N (Hampton Research). Data were integrated using Bruker SAINT software.[20] Data were subsequently corrected for absorption by the program SADABS.[21] The space group determinations and tests for merohedral twinning were carried out using XPREP.[22] In all cases, the highest possible space group was chosen. All structures were solved by direct methods and refined using the SHELXTL 97 software suite.[23] Atoms were located from iterative examination of difference *F*-maps following least-squares refinements of the earlier models. Hydrogen atoms were placed in calculated positions and included as riding atoms with isotropic displacement parameters 1.2−1.5 times U_{eq} of the attached C atoms. Data were collected at 298(2) K for Cu-TBA-1, -2, and -2F reported in this paper. All structures were examined using the ADDSYM subroutine of PLATON[24] to ensure that no additional symmetry could be applied to the models. All ellipsoids in ORTEP diagrams are displayed at the 50% probability level unless noted otherwise. Supporting Information contains a detailed data collection strategy and crystallographic data for the three MOFs reported in this paper. Crystal data and details of data collection, structure solution and refinement are summarized in Supporting Information, Tables S1, S2, and S3. Crystallographic data (excluding structure factors) for the structures reported in this paper have been deposited with the Cambridge Crystallographic Data Centre (CCDC) as deposition Nos. CCDC 811812−811814. Copies of the data can be obtained, free of charge, on application to the CCDC, 12 Union Road, Cambridge CB2 lEZ, U.K. (fax: + 44 (1223) 336 033; e-mail: deposit@ccdc.cam.ac.uk).

Gas Adsorption Measurements. Low pressure volumetric gas adsorption measurements involved in this work were performed at 77 K for H_2 and N_2, maintained by a liquid nitrogen bath, with pressures ranging from 0 to 760 Torr on a Quantachrome Quadrasorb automatic volumetric instrument, while CO_2 adsorption measurements were done at room temperature (298 K) with the same pressures range. In all adsorption measurements, ultra high-purity H_2 was obtained by using calcium aluminosilicate adsorbents to remove trace amounts of water and other impurities before introduction into the system. The blue colored micro crystals of each MOF were soaked in 1:1 dry dichloromethane and methanol mixture for 12 h. Fresh 1:1 dry dichloromethane and methanol mixture was subsequently added, and the crystals were allowed to stay for an additional 48 h to remove coordinated and free solvates (DMF and EtOH) present in framework. The sample was dried under a dynamic vacuum ($<10^{-3}$ Torr) at room temperature overnight. The coordinated solvents DMF and EtOH on the secondary binding units (SBUs) remain in the framework at this stage. To remove coordinated solvents, samples were heated at 60 °C for 12 h and 100 °C for 12 h under a dynamic vacuum. Upon heating also, Cu-TBA-1, -2, and -2F retain their framework (See Supporting Information).

Simulation Model and Methods. Grand canonical Monte Carlo (GCMC) simulations were carried out for H_2 adsorption in Cu-TBA-2 and -2F to unravel the effect of fluorine atoms on adsorption and to identify the adsorption sites in gas-loaded structures. The experimentally determined desolvated crystal structures were used in the simulations. The porosities of Cu-TBA-2 and -2F are 0.540 and 0.531, respectively, evaluated using Materials Studio[25] with a Connolly probe radius equal to zero. The H_2 molecule was represented as a two-site rigid molecule with H−H bond length of 0.74 Å.[26] The dispersion interactions of the framework atoms in Cu-TBA-2 and -2F were modeled by the Universal Force Field (UFF).[27] The Lorentz−Berthelot combining rules were used to calculate the cross Lennard−Jones (LJ) interaction parameters. GCMC simulations were conducted for H_2 adsorption in Cu-TBA-2 and -2F at 77 K. The LJ interactions were evaluated using a spherical cutoff with the long-range corrections added. Five types of trial moves were conducted for H_2 molecules, namely, displacement, rotation, partial regrowth at a neighboring position, complete regrowth at a new position, and swap with the reservoir. The number of trial moves in the simulations

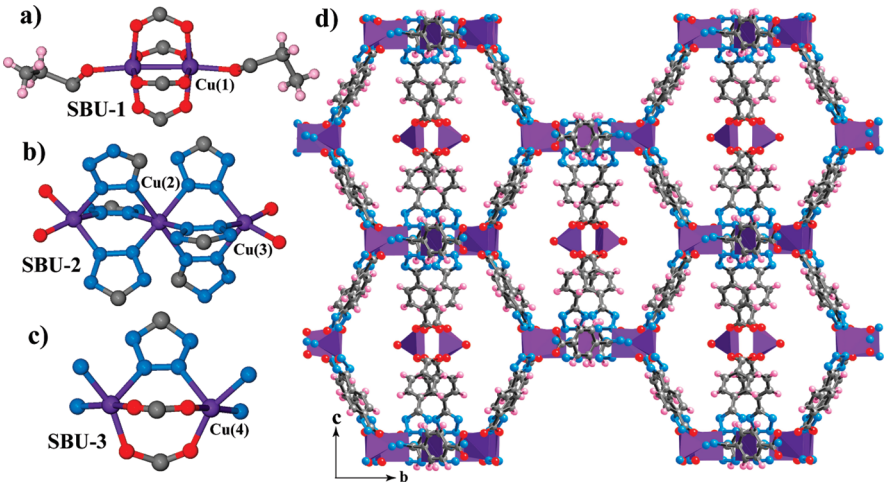

Figure 1. Schematic drawing for crystal structure of $Cu_9(4\text{-TBA})_{10}(EtOH)_2$ (**Cu-TBA-1**). (a) Octahedral paddlewheel type SBU-1 (6 oxygen) along with 2 axial solvent molecules. (b) SBU-2 with octahedral Cu(II) (middle, coordinated to 6 nitrogen) surrounded by two trigonal bipyramidal Cu(II) (coordinated to 3 nitrogen and 2 oxygen). (c) Trigonal bipyramidal SBU-3 where Cu(II) is coordinated to 3 nitrogen and 2 oxygen. (d) Packing diagram showing formation of hollow cages formation through *a* axis. Solvent molecules are omitted for clarity. Color code: Cu (magenta), N (blue), O (red), C (black), H (pink).

was 2×10^7. The first 10^7 moves were used for equilibration and the subsequent 10^7 moves for production.

RESULT AND DISCUSSION

Synthesis. In the present manuscript, we have used 4-TBA and its partially fluorinated analogue 2-F-4-TBA as key links and presented a comparative study toward their gas adsorption properties. We chose tetrazole benzoic acids as the ligand for this study for the following reasons. (a) They possesses two functional groups with different coordination modes. The carboxylate and tetrazole group can adopt versatile coordination conformations, from monodentate to tetradentate. Combination of both these functionalities can create a number of new MOFs with uncommon topologies. (b) The elongated structure of the ligand with carboxylate and tetrazole functionality can create large pores for gas adsorption. We will discuss the structural details of Cu-TBA-1, -2, and -2F respectively.

Crystal Structure of Cu-TBA-1. In the crystal structure of Cu-TBA-1, three types of SBUs are present, where the Cu(II) metal centers are either in octahedral (SBU-1 and -2) or in trigonal bipyramidal coordination state (SBU-2 and −3). It is noteworthy that, octahedral metal centers [Cu(1) and Cu(2)] in the SBU-1 and -2 are coordinated exclusively to oxygen or nitrogen; while trigonal bipyramidal metal centers [Cu(3) and Cu(4)] are coordinated to both oxygen and nitrogen (Figure 1). Among the three SBUs, SBU-1 is a Cu paddlewheel type, where four μ_2-OCO^- carboxyl groups from different 4-TBA ligands join to two different Cu(II) atoms. Two axial positions of Cu(II) are coordinated by EtOH molecules as shown in Figure 1a and Scheme 1. Removing coordinated solvent molecules from the paddlewheel SBU via solvent exchange followed by evacuation at elevated temperature can create open metal sites. In SBU-2, there are two types Cu(II) atoms in which Cu(2) is coordinated to four different μ_2-tetrazolyl and two different μ_4-tetrazolyl nitrogen. On the other hand, Cu(3) is coordinated to two nitrogen from two different μ_2-tetrazolyl groups, one nitrogen from μ_4-tetrazolyl group and two oxygens from carboxylate functionality of 4-TBA ligand (Figure 1b). Similarly the SBU-3 is formed by

Scheme 1. Schematic Drawing and Mode of Coordination of TBA Links Observed in Cu-TBA-1, -2, and -2F[a]

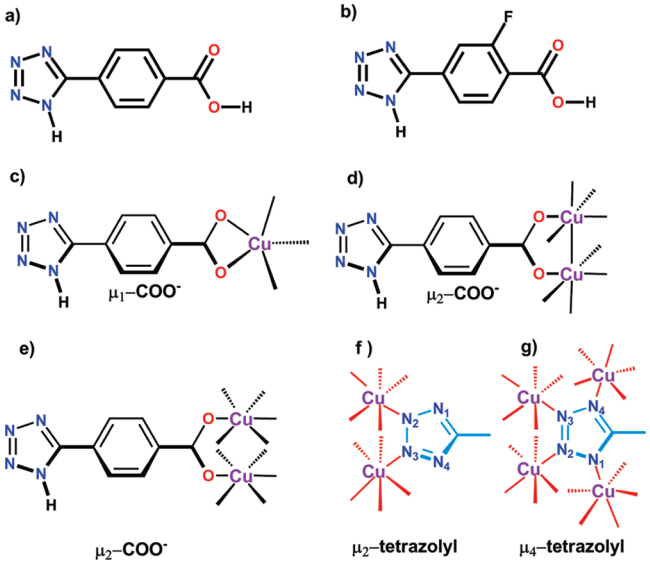

[a] (a) Schematic drawing of 4-(1*H*-tetrazole-5-yl)benzoic acid or 4-tetrazole benzoic acid (**4-TBA**). (b) Schematic drawing of 2-fluoro-4-(1*H*-tetrazole-5-yl)benzoic acid or 2-fluoro-4-tetrazole benzoic acid (**2F-4-TBA**). (c) μ_1-COO^- coordination mode for carboxylic group. (d) μ_2-COO^- coordination mode for carboxylic group with paddlewheel SBU. (e) μ_2-tetrazolyl coordination mode for carboxylic group. (f) μ_2-tetrazolyl coordination mode for tetrazolyl group. (g) μ_4-tetrazolyl coordination mode for tetrazolyl functionality.

coordination of three different μ_2-tetrazolyl, one μ_4-tetrazolyl nitrogen, and two μ_2-OCO carboxylate functionality to Cu(4) as shown in Figure 1c. In the crystal structure of Cu-TBA-1, the paddlewheel type SBU-1 extends in three dimensions through its μ_2-tetrazolyl group along *a* and *c* axis connecting to SBU-2 as shown in Figure 1b and 1d. Further, SBU-2 expands its coordination sphere along the *ab* plane connecting it is both sides to the

dx.doi.org/10.1021/cm2004352 |*Chem. Mater.* 2011, 23, 2908–2916

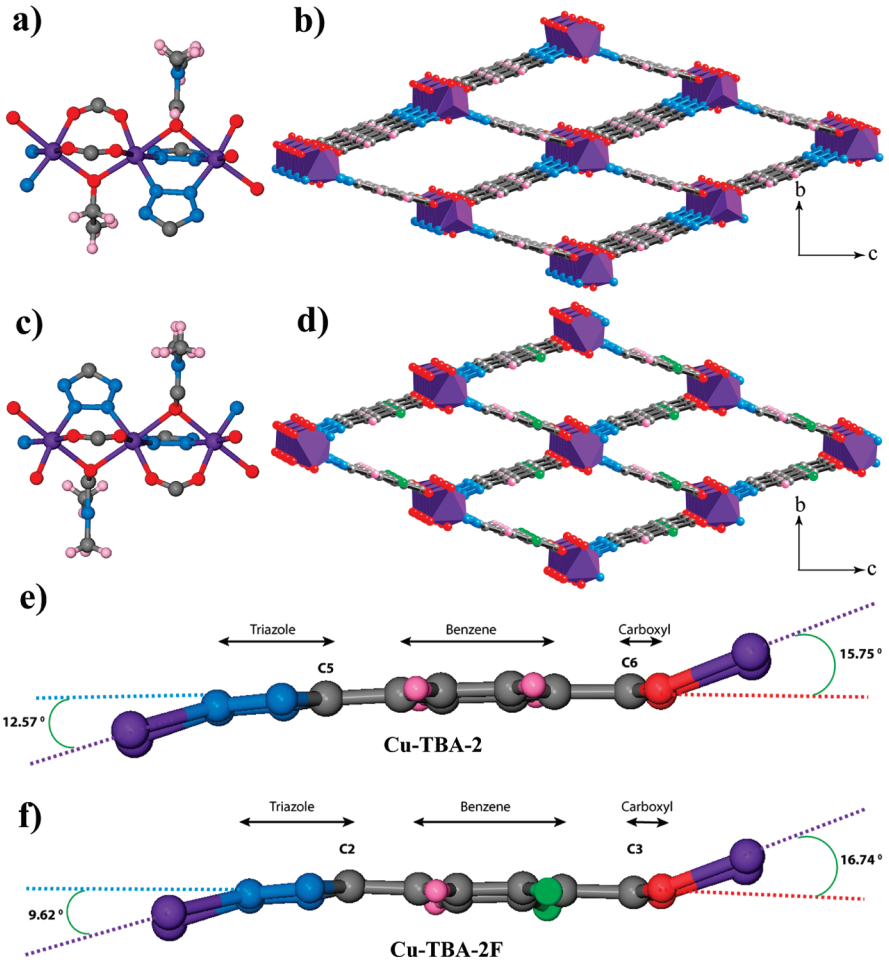

Figure 2. Schematic drawing and structural deformation for crystal structure of $Cu_2(4\text{-TBA})_2(DMF)(EtOH)$ (**Cu-TBA-2**) and Cu_2 $(2F\text{-}4\text{-TBA})_2(DMF)2$ (**Cu-TBA-2F**). (a) Octahedral Cu(II) SBU in Cu-TBA-2 coordinated to 4 oxygen and 2 nitrogen. (b) Packing diagram showing formation of one-dimensional pores through *a* axis for Cu-TBA-2. (c) Octahedral Cu(II) SBU in Cu-TBA-2F coordinated to 4 nitrogen and 2 oxygen. (d) Packing diagram showing formation one-dimensional pores and pointing fluorine atoms into the pores through *a* axis for Cu-TBA-2F. (e) Formation of 12.57° and 15.75° angle between tetrazole ring with benzene ring plane and carboxyl group with benzene ring plane, respectively Cu-TBA-2. (f) Formation of 9.62° and 6.74° angles between the tetrazole ring with the benzene ring plane and the carboxyl group with the benzene ring plane, respectively, in Cu-TBA-2F, showing variation in angle formation due to the effect of the protruding fluorine. Color code: Cu (magenta), N (blue), O (red), C (black), H (pink), and F (green).

SBU-3, and thus creates a three-dimensional architecture (Supporting Information, Figure S16).

Cu-TBA-1 forms a highly connected porous structure because of the different binding modes of the 4-TBA ligand. In the crystal structure, three types of SBUs with two different types of bridging modes for the tetrazolyl group and the carboxyl group give a highly connected structure with large cages of 18.4 × 19.7 Å outer dimensions, with 11.6 Å pore radii inside it (Figure 1d and Supporting Information, Figure S17). These pores are accessible for gas adsorption as they have the pore aperture of 3.641 Å. The paddlewheel type SBU-1 forms the wall of cages, and two solvent molecules attached to it protrude into the pores, which can be removed after evacuation for creation of large void space. The solvent accessible volume calculated for guest free Cu-TBA-1 using PLATON is as high as 51.5%. The structure of Cu-TBA-1 is highly stable until 230 °C and maintains crystallinity at higher temperature as well.

Crystal Structure of Cu-TBA-2. In the crystal structure of Cu-TBA-2, only one SBU has been observed with octahedral Cu(II) centers. In Cu-TBA-2, two oxygen atoms from μ_2-OCO carboxylate groups are coordinated to two adjacent Cu(II) centers. These Cu(II) centers are also connected to four nitrogen atoms from ditopic μ_2-tetrazolyl groups. One oxygen atom from DMF and one oxygen atom from EtOH are coordinated to these Cu centers to form an octahedral environment as shown in Figure 2a and Scheme 1. The structure of Cu-TBA-2 extends in the *ab* plane through the coordination of Cu(II) centers, ditopic tetrazolyl groups, and DMF or EtOH in alternate fashion (Supporting Information, Figure S18). The joining of these carboxyl and tetrazolyl groups in ditopic fashion along the *c* axis creates one-dimensional square shaped pores of 4.24 Å, where bridging disordered DMF and EtOH are pointing toward the pores (Figure 2b and Supporting Information, Figure S19).

Crystal Structure of Cu-TBA-2F. In the crystal structure of Cu-TBA-2F, only one type SBU has been observed (like Cu-TBA-2) with octahedral Cu(II) metal center. In the SBU of Cu-TBA-2F, two oxygen atoms from μ_2-OCO carboxylate groups, two nitrogen atoms from ditopic μ_2-tetrazolyl groups, and two DMF molecules are coordinated to the two adjacent Cu centers to form the octahedral Cu(II) centers as shown in Figure 2c and

dx.doi.org/10.1021/cm2004352 |*Chem. Mater.* 2011, 23, 2908–2916

Scheme 1. Each Cu(II) atoms in the structure is connected through carboxyl and tetrazolyl groups along the *a* axis. The structure of Cu-TBA-2 extends in the *ab* plane through joining of μ_2-carboxyl and ditopic tetrazolyl groups in alternate ditopic fashion (Supporting Information, Figure S20) and creates the one-dimensional, square shaped pores of 3.626 Å along the *a* axis (Figure 2d). In Cu-TBA-2 and -2F, both tetrazolate ring and carboxyl functionality adopt a bend conformation (Figure 2e and 2f). The tetrazolate ring for Cu-TBA-2 and -2F adopts an angle of 12.57° and 9.62° with respect to the plane of the benzene ring, while 15.75° and 16.74° are the angles for the carboxyl group (Figure 2f). In Cu-TBA-2F, because of the steric hindrance of fluorine atom with solvent molecules, the bending angle increases from 15.75° to 16.74° for the coordinated carboxyl group. Because of the higher bending of carboxyl group, the pores formed in Cu-TBA-2F have smaller dimensions (3.52 Å) than Cu-TBA-2 (4.24 Å) (Supporting Information, Figure S21). Structures of Cu-TBA-2 and -2F are very similar in nature, well simplified compared to Cu-TBA-1, and porous. The solvent accessible void calculated for the solvent free Cu-TBA-2 and -2F using PLATON are 10.2% and 8.4%, respectively. In the crystal structure of the Cu-TBA-2F, fluorine atoms are protruding in the pores, leading to the pore blockage and decreasing the solvent accessible volume.

Structural analysis of Cu-TBA-1, -2, and -2F reveals several interesting features. Cu-TBA-1 is highly porous and highly connected MOF with different connectivity's for tetrazolate (μ_2-tetrazolyl, μ_4-tetrazolyl) as well as carboxyl group (μ_2-OCO^-, μ_2-OCO^-). The Cu-TBA-1 has large elliptical cages possessing large pores of about 11.664 Å. On the other hand Cu-TBA-2, the structural isomer of Cu-TBA-1 is well simplified and contains only one octahedral SBU with μ_2-tetrazolyl group and μ_2-OCO^- group. The structure of Cu-TBA-2F is iso-structural to Cu-TBA-2 in terms of connectivity of the SBU and formation of the extended 3D structure. In this structure, because of insertion of highly electronegative fluorine atom into the system, bending of the carboxyl group increases from 15.75 Å to 16.74 Å from the benzene ring plane, possibly because of the interaction of fluorine atoms with neighboring atoms resulting in the formation of smaller pores of 3.526 Å as compared to the Cu-TBA-2. Moreover, in the structure of Cu-TBA-2F, uncoordinated exposed fluorine atoms protrude into the pores resulting in pore blockage.

Thermal Stability and PXRD Analysis. We have prepared the Cu-TBA-1, -2, and -2F at the gram scale to allow detailed investigation of the aforementioned properties and to examine the architectural and thermal stability reported in this paper. Thermal gravimetric analysis (TGA) performed on as-synthesized Cu-TBA-1, -2, and -2F revealed that these compounds have high thermal stability (see Section S4 in Supporting Information, for all data and interpretations regarding guest mobility and thermal stability of these MOFs). The TGA trace for as synthesized Cu-TBA-1, -2, and -2F showed a gradual weight-loss step of 22.5% (20−200 °C), 3.25% (20−200 °C), and 3.0% (20−200 °C) respectively corresponding to escape of coordinated *N,N* dimethylformamide (DMF) and EtOH and guest solvent molecules in pores. This is followed by a sharp weight loss (200−390 °C) probably because of the decomposition of the framework. It is noteworthy that the TGA traces solvent exchanged Cu-TBA-2 show a larger weight loss of 12.5% (20−200 °C) corresponding to escape of coordinated DMF, EtOH, and non-coordinated guest solvent molecules in pores (Supporting Information, Figure S13). However, the same for Cu-TBA-2F does not change its TGA behavior in large extent [6.5% (20−200 °C)]. A possible reason for this could be due to difficulty of removal of coordinated DMF and EtOH molecules form Cu-TBA-2F framework (Supporting Information, Figure S15).

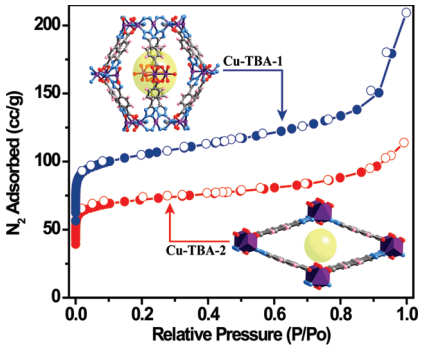

Figure 3. N_2 adsorption isotherms below 1.0 bar for Cu-TBA-1 (blue) and Cu-TBA-2 (red) at 77 K. Filled and open circles represent adsorption and desorption data, respectively. Pores available for N_2 gas adsorption in the Cu-TBA-1 and -2 are shown with a yellow ball in the inset.

To confirm the phase purity of the bulk materials, powder X-ray diffraction (PXRD) experiments were carried out on all complexes. All major peaks of experimental PXRDs of Cu-TBA-1, -2, and -2F match well with simulated PXRDs, indicating their reasonable crystalline phase purity[28] (Supporting Information, Figure S1 to S4). We have performed in situ variable temperature PXRD (VT-PXRD) of Cu-TBA-1, -2, and -2F to understand the structural changes at high temperature (Supporting Information, Figure S5 to S7). In situ VT-PXRD patterns of Cu-TBA-1, -2, and -2F have been collected at different temperatures that coincide with the patterns simulated from single crystal structures. In situ VT-PXRD of all MOFs reported here indicate the stability and retention of crystallinity of these samples (230 °C) at high temperature. It also reveals that there are no possibilities of phase changes at higher temperature for these samples. Small differences in the intensities of the reflections are observed at higher temperatures because of the removal of residual solvent molecules.

Gas Adsorption Measurements. The permanent porosity of Cu-TBA-1, -2, and -2F is confirmed by gas adsorption studies. The N_2 adsorption isotherms of the activated sample of Cu-TBA-1 exhibit type-I sorption behavior (Figure 3) with a Langmuir and Brunauer−Emmett−Teller (BET) surface area of 686 m^2/g and 616 m^2/g respectively. The activated sample of Cu-TBA-2 also shows type-I sorption behavior with 402 m^2/g (Langmuir) and 356 m^2/g (BET) surface areas respectively. These results are justified as Cu-TBA-2 has less pore size (4.24 Å), low void space, and less solvent accessible volume (10.9%) as compared to Cu-TBA-1 (51.3%). Although Cu-TBA-2 and -2F are iso-structural in terms of the connectivity of the SBU and formation of an extended 3D structure, Cu-TBA-2F is nonporous to N_2 adsorption. The total reduction of surface area in Cu-TBA-2F is presumably due to the insertion of fluorine and subsequently inaccessibility of pores. Fluorine atom has considerably higher van der Waals radius (1.47 Å) than H_2 (1.20 Å). Also, as mentioned previously the coordinated guest solvents present in the framework of Cu-TBA-2F are difficult to remove from the framework possibly because of the highly electronegative nature of fluorine atom. The kinetic diameter of N_2 (3.65 Å) is higher than the pore size of Cu-TBA-2F (3.52 Å), and the low kinetic energy of the N_2 molecules at 77 K result in N_2 molecules being

dx.doi.org/10.1021/cm2004352 |*Chem. Mater.* 2011, 23, 2908–2916

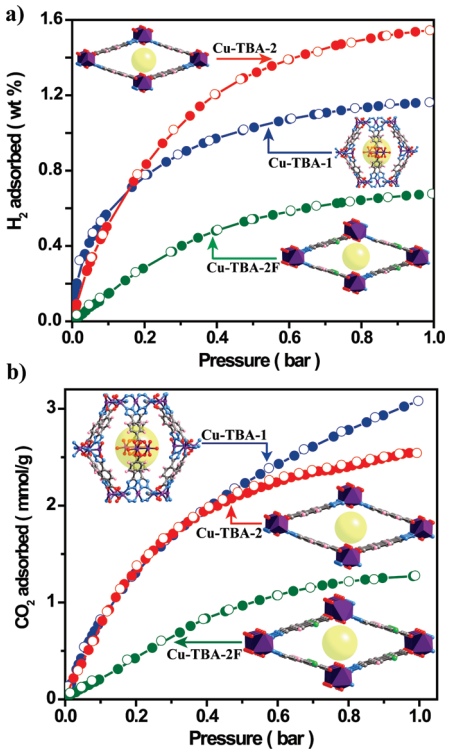

Figure 4. (a) H_2 adsorption isotherms below 1.0 bar for Cu-TBA-1 (blue), -2 (red), and -2F (green) at 77 K. Filled and open circles represent adsorption and desorption respectively. Pores available for H_2 gas adsorption in Cu-TBA-1, -2, and -2F are shown with a yellow ball in the inset. (b) CO_2 adsorption isotherms below 1.0 bar for Cu-TBA-1 (blue), -2 (red), and -2F (green) at 298 K. Filled and open circles represent adsorption and desorption data, respectively. Pores available for CO_2 gas adsorption in Cu-TBA-1, -2, and -2F are shown with a yellow ball in the inset.

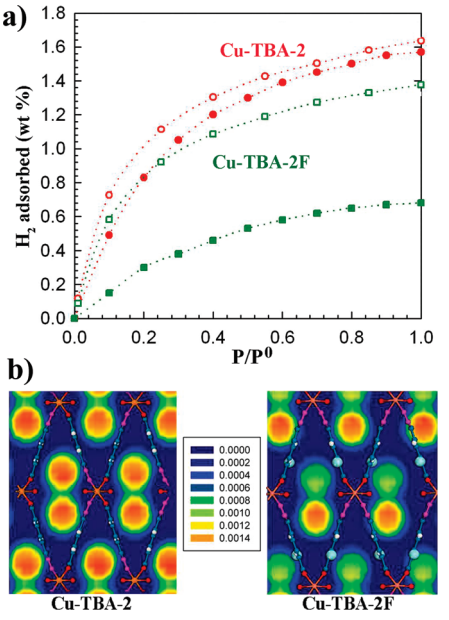

Figure 5. Simulated adsorption isotherms and H_2 adsorption sites in Cu-TBA-2 and -2F. (a) Simulated and experimental adsorption isotherms of H_2 in Cu-TBA-2 (red) and -2F (green) at 77 K. The open symbols are from simulation and the filled symbols are from experimental data. (b) H_2 adsorption density contours in Cu-TBA-2 and -2F at 1 kPa.

unable to effectively enter small pores of Cu-TBA-2F. However, Cu-TBA-2F is able to take up H_2 (2.89 Å) and CO_2 (3.4 Å) as it has the less kinetic diameter.

The H_2 and CO_2 adsorption properties of Cu-TBA-1, -2, and -2F are shown in Figure 4. All these MOFs show reversible type-I H_2 and CO_2 adsorption isotherms at 77 K and 298 K respectively. In addition, the absence of adsorption−desorption hysteresis indicates that H_2 and CO_2 is reversibly adsorbed by all the MOFs reported here. At 760 Torr and 77 K, Cu-TBA-1 and -2 adsorbs 1.16 and 1.54 wt % H_2, while Cu-TBA-2F adsorbs 0.67 wt % H_2. The difference between the H_2 uptakes of Cu-TBA-1 and -2 is well anticipated as small pores of Cu-TBA-2 are more suitable for H_2 adsorption which is well supported by previous reports.[29] Fluorine atoms protrude into the pores in the case of Cu-TBA-2F; as a result because of decreased pore size and steric crowding, it shows less adsorption capacity for H_2. The CO_2 adsorption properties of Cu-TBA-1, -2, and -2F are shown in Figure 4b. Cu-TBA-1 and -2 adsorbs 3.08 and 2.54 mmol/g, while Cu-TBA-2F adsorbs 1.27 mmol/g of CO_2 at 298 K and 1 bar pressure. This reversible H_2 and CO_2 uptake at 1 atm pressure is comparable with previously reported ZIFs and well-known MOFs materials (see Section S5 in Supporting Information, for a detailed comparison of high H_2 and CO_2 uptake in MOFs).[30] The prominent difference in CO_2 uptake properties between the Cu-TBA-1 and -2 is well-defined. As shown in Figure 4b, at low pressure up to 0.45 bar both these MOFs adsorb CO_2 equally as Cu-TBA-1 and -2 have availability of adsorptive pores until that pressure. After 0.45 bar pressure, Cu-TBA-2 adsorbs less CO_2 gas as its pore size is less than that of Cu-TBA-1. The larger pores of Cu-TBA-1 adsorb more CO_2 as pressure increases from 0.45 to 1 bar. The availability of larger and suitable pores for CO_2 adsorption in Cu-TBA-1 over Cu-TBA-2 gives more adsorption capacity in it. Again as discussed earlier, because of blocking of pores, Cu-TBA-2F adsorbs less amount of CO_2, although it is iso-structural, in terms of the connectivity of the SBU and formation of extended 3D structure with Cu-TBA-2.

Simulation Results. The H_2 adsorption isotherms in Cu-TBA-2 and -2F at 77 K from simulation are shown in Figure 5a. The simulated H_2 adsorption agrees fairly well with experiment in Cu-TBA-2. Specifically, the adsorption at 1 bar is 1.54 wt % from experiment and 1.62 wt % predicted by simulation. But the simulated isotherm in Cu-TBA-2F largely overestimates experimental data as the simulated adsorption is 1.36 wt % whereas the experimental is 0.67 wt %. The deviations between experimental and simulation isotherms in Cu-TBA-2F are much larger than in Cu-TBA-2. This is possibly attributed to the interactions of protruding fluorine atoms in Cu-TBA-2F and difficulties in removing the coordinated guest solvent molecules from the pores. At low pressures, both the simulated isotherms in Cu-TBA-2 and -2F are nearly similar, because of the availability of smaller pores in both MOFs. But as we move further to high pressures, because of the inaccessibility of pores for H_2 adsorption in Cu-TBA-2F over Cu-TBA-2, lower H_2 adsorption is observed in Cu-TBA-2F.

To identify the favorable binding sites for H_2 in Cu-TBA-2 and -2F, the density distributions of adsorbed H_2 molecules at 77 K and 1 kPa were estimated along the *YZ* plane. As illustrated in Figure 5b, H_2 molecules are primarily adsorbed in the pores along the *X* axis, and the binding sites are mostly located in the

dx.doi.org/10.1021/cm2004352 |*Chem. Mater.* 2011, 23, 2908–2916

pore centers in both Cu-TBA-2 and -2F. More specifically, the density in Cu-TBA-2 equally distributes in the middle of the pores as the protruding hydrogen atoms from ligand do not have a strong effect on adsorbed H_2 gas molecules. The density in Cu-TBA-2F is lower, however, particularly in the regions near the fluorine atoms because of steric hindrance.

CONCLUSION

In conclusion, we have synthesized solvothermally three new 3D MOFs using the predesigned 4-TBA and 2-F-4-TBA ligands with a transition metal center Cu(II). These MOFs are highly porous and show high adsorption capacity for N_2, H_2, and CO_2 at 1 atm pressure. At 1 atm pressure, Cu-TBA-1 shows 1.16 wt % H_2 and 3.08 mmol/g CO_2 uptake; while Cu-TBA-2 shows uptake of 1.54 wt % H_2 and 2.54 mmol/g CO_2 at 77 and 298 K. These MOFs are highly stable and retain crystallinity until 230 °C which was confirmed by TGA and in situ VT-PXRD patterns. The phenomenon of structural isomerism has been observed in the Cu-TBA-1 and Cu-TBA-2 upon changing metal source during synthesis. Also iso-structural Cu-TBA-2 and Cu-TBA-2F were obtained by changing the ligand 4-TBA to 2-F-4-TBA. Here, direct comparison between iso-structural partially fluorinated Cu-TBA-2F and nonfluorinated Cu-TBA-2 suggested that enhancement of H_2 adsorption due to fluorination in MOFs is not an universal phenomenon, but it is rather system specific and can differ from system to system. The density distributions of adsorbed H_2 molecules in Cu-TBA-2 and -2F from simulation suggest that H_2 molecules are primarily adsorbed in the pores along the *X* axis and the binding sites are mostly located in the pore centers. Based on the simulation, protruding fluorine atoms from 2-F-4-TBA appear to cause a steric hindrance and a lower adsorption for H_2. Nevertheless, thorough research work is necessary on H_2 adsorption on iso-structural fluorinated/non-fluorinated MOFs before we can conclusively indicate a positive/negative effect of fluorination on enhancement of hydrogen adsorption in MOFs.

ASSOCIATED CONTENT

Supporting Information. Description of experimental details, including synthetic methods, crystallography, supplementary figures, including TGA, infrared spectroscopy, powder XRD profiles, tables of crystallographic data, CIF files, and anisotropic thermal ellipsoids for MOFs reported in this paper. This material is available free of charge via the Internet at http://pubs.acs.org.

AUTHOR INFORMATION

Corresponding Author

*E-mail: r.banerjee@ncl.res.in. Fax: + 91-20-25902636. Phone: + 91-20-25902535.

ACKNOWLEDGMENT

P.P. acknowledges CSIR for a project assistantship (PA-II) from CSIR's XIth Five Year Plan Project (NWP0022-H). R.B. acknowledges Dr. S. Pal, Director NCL for in house project (MLP020626) and CSIR's XIth Five Year Plan Project (NWP0022-H) and Clean Coal Technology Project (NWP0021-A) for funding and also Dr. B. D. Kulkarni, Dr. S. Sivaram, and Dr. K. Vijaymohanan for their encouragement. Financial assistance from the DST (SR/S1/IC-22/2009) is acknowledged.

REFERENCES

(1) (a) Janiak, C. *J. Chem. Soc., Dalton Trans.* **2003**, 2781. (b) Moulton, B.; Zaworotko, M. J. *Chem. Rev.* **2001**, *101*, 1629. (c) Eddaoudi, M.; Moler, D. B.; Li, H.; Chen, B.; Reineke, T. M.; O'Keeffe, M.; Yaghi, O. M. *Acc. Chem. Res.* **2001**, *34*, 319. (d) Robson, R. *J. Chem. Soc., Dalton Trans.* **2000**, 3735. (e) Yaghi, O. M. *Nat. Mater.* **2007**, *6*, 92. (f) Georgiev, I. G.; MacGillivray, L. R. *Chem. Soc. Rev.* **2007**, *36*, 1239. (g) Corma, A.; Garcia, H.; Xamena, F. X. L. *Chem. Rev.* **2010**, *110*, 4606. (h) James, S. L. *Chem. Soc. Rev.* **2003**, *32*, 276. (i) Yaghi, O. M.; Li, H.; Davis, C.; Richardson, D.; Groy, T. L. *Acc. Chem. Res.* **1998**, *31*, 474. (j) Janiak, C. *Angew. Chem., Int. Ed. Engl.* **1997**, *36*, 1431. (k) Blake, A. J.; Champness, N. R.; Hubberstey, P.; Li, W.-S.; Withersby, M. A.; Schroder, M. *Coord. Chem. Rev.* **1999**, *183*, 117. (l) Kesanli, B.; Cui, Y.; Smith, M.; Bittner, E.; Bockrath, B.; Lin, W. *Angew. Chem., Int. Ed.* **2005**, *44*, 72.

(2) The DOE targets for the gravimetric and volumetric system for near-ambient temperature (from −40 to 85 °C) and moderate pressure (less than 100 bar) are 6.0 wt % (45 g/L) for the year 2010 and 9.0 wt % (81 g/L) for 2015. (a) DOE Office of Energy Efficiency and Renewable Energy Hydrogen, Fuel Cells & Infrastructure Technologies Program Multi-Year Research, Development and Demonstration Plan, available at http://www.eere.energy.gov/hydrogenandfuelcells/mypp. (b) FY 2006 Annual Progress Report for the DOE Hydrogen Program, Nov 2006, available at http://www.hydrogen.energy.gov/annual_progress.html. (c) Satyapal, S.; et al. FY 2006 DOE Hydrogen Program Annual Merit Review and Peer Evaluation Meeting Proceedings, Plenary Session, available at http://www.hydrogen.energy.gov/annual_review06_plenary.html.

(3) (a) Dillon, A. C.; Jones, K. M.; Bekkedahl, T. A.; Kiang, C. H.; Bethune, D. S.; Heben, M. J. *Nature* **1997**, *386*, 377. (b) Liu, C.; Fan, Y. Y.; Liu, M.; Cong, H. T.; Cheng, H. M.; Dresselhaus, M. S. *Science* **1999**, *286*, 1127. (c) Chambers, A.; Park, C.; Baker, R. T. K.; Rodriguez, N. M. *J. Phys. Chem. B* **1998**, *102*, 4253. (d) Chen, P.; Wu, X.; Lin, J.; Tan, K. L. *Science* **1999**, *285*, 91. (e) Huang, T. *Nanotechnology That Will Change the World*; Enlighten Noah Publishing: 2002, p 38.

(4) (a) Li, Y.; Yang, R. T. *J. Phys. Chem. B* **2006**, *110*, 17175. (b) Nijkamp, M. G.; Raaymakers, J. E.; van Dillen, A. J.; de Jong, K. P. *Appl. Phys. A: Mater. Sci. Process.* **2001**, *72*, 619. (c) Darkrim, F.; Aoufi, A.; Malbrunot, P.; Levesque, D. *J. Chem. Phys.* **2000**, *112*, 5991.(d) Yang, R. T. *Adsorbents: Fundamentals and Applications*; Wiley: New York, 2003, 280.

(5) (a) Hynek, S.; Fuller, W.; Bentley, J. *Int. J. Hydrogen Energy* **1997**, *22*, 601. (b) Carpetis, C.; Peschka, W. *Int. J. Hydrogen Energy* **1980**, *5*, 539. (c) Noh, J. S.; Agarwal, R. K.; Schwarz, J. A. *Int. J. Hydrogen Energy* **1987**, *12*, 693. (d) Chahine, R.; Bose, T. K. *Int. J. Hydrogen Energy* **1994**, *19*, 161. (e) Zhou, Y.; Zhou, L. *Sci. China, Ser. B* **1996**, *39*, 598. (f) Wang, Q.; Johnson, J. K. *J. Chem. Phys.* **1999**, *110*, 577. (g) de la Casa-Lillo, M. A.; Lamari-Darkrim, F.; Cazorla-Amoros, D.; Linares-Solano, A. *J. Phys. Chem. B* **2002**, *106*, 10930. (h) Wang, H.; Gao, Q.; Hu, J. *J. Am. Chem. Soc.* **2009**, *131*, 7016.

(6) (a) Das, L. M. *Int. J. Hydrogen Energy* **1996**, *21*, 789.(b) Fukai, Y. In *The Metal−Hydrogen System*; Gonser, U., Ed.; Springer Series in Material Science; Springer-Verlag: New York, 1993. (c) Imamura, H.; Sakasai, N. *J. Alloys Compd.* **1995**, *231*, 810. (d) Gross, K. J.; Spatz, P.; Züttel, A.; Schlapbach, L. *J. Swiss Soc. Surf. Mater.* **1996**, *5*, 22. (e) Imamura, H.; Sakasai, N.; Kajii, Y. *J. Alloys Compd.* **1996**, *232*, 218. (f) Imamura, H.; Sakasai, N.; Fujinaga, T. *J. Alloys Compd.* **1997**, *253−254*, 34. (g) Sandrock, G. *J. Alloys Compd.* **1999**, *293*, 877. (h) Schuth, F.; Bogdanovi, B.; Felderhoff, M. *Chem. Commun.* **2004**, 2249.

(7) (a) Eddaoudi, M.; Kim, J.; Rosi, N.; Vodak, D.; Wachter, J.; O'Keeffe, M.; Yaghi, O. M. *Science* **2002**, *295*, 469. (b) Kitagawa, S.; Kitaura, R.; Noro, S.-I. *Angew. Chem., Int. Ed.* **2004**, *43*, 2334. (c) Matsuda, R.; Kitaura, R.; Kitagawa, S.; Kubota, Y.; Belosludov, R. V.; Kobayashi, T. C.; Sakamoto, H.; Chiba, T.; Takata, M.; Kawazoe, Y.; Mita, Y. *Nature* **2005**, *436*, 238. (d) Millward, A. R.; Yaghi, O. M. *J. Am.*

Chem. Soc. **2005**, *127*, 17998. (e) Furukawa, H.; Miller, M. A.; Yaghi, O. M. *J. Mater. Chem.* **2007**, *17*, 3197. (f) Ferey, G. *Chem. Soc. Rev.* **2008**, *37*, 191. (g) Morris, R. E.; Wheatley, P. S. *Angew. Chem., Int. Ed.* **2008**, *47*, 4966. (h) Llewellyn, P. L.; Bourrelly, S.; Serre, C.; Vimont, A.; Daturi, M.; Hamon, L.; De Weireld, G.; Chang, J.-S.; Hong, D.-Y.; Hwang, Y. K.; Jhung, S. H.; Ferey, G. *Langmuir* **2008**, *24*, 7245. (i) Murray, L. J.; Dinca, M.; Long, J. R. *Chem. Soc. Rev.* **2009**, *38*, 1294. (j) Chen, B.; Xiang, S.; Qian, G. *Acc. Chem. Res.* **2010**, *43*, 1115.

(8) (a) Deng, H.; Doonan, C. J.; Furukawa, H.; Ferreira, R. B.; Towne, J.; Knobler, C. B.; Wang, B.; Yaghi, O. M. *Science* **2010**, *327*, 846. (b) Koh, K.; Wong-Foy, A. G.; Matzger, A. J. *J. Am. Chem. Soc.* **2009**, *131*, 4184. (c) Zhao, D.; Yuan, D.; Sun, D.; Zhou, H. C. *J. Am. Chem. Soc.* **2009**, *131*, 9186. (d) Furukawa, H.; Ko, N.; Go, Y. B.; Aratani, N.; Choi, S. B.; Choi, E.; Yazaydin, A. O.; Snurr, R. Q.; O'Keeffe, M.; Kim, J.; Yaghi, O. M. *Science* **2010**, *329*, 427. (e) Ma, L.; Abney, C.; Lin, W. *Chem. Soc. Rev.* **2009**, *38*, 1248. (f) Evans, O. R.; Ngo, H. L.; Lin, W. *J. Am. Chem. Soc.* **2001**, *123*, 10395.

(9) (a) Chen, B.; Eddaoudi, M.; Hyde, S. T.; O'Keeffe, M.; Yaghi, O. M. *Science* **2001**, *291*, 1021. (b) Lin, X.; Jia, J.; Hubberstey, P.; Schröder, M.; Champness, N. R. *CrystEngComm* **2007**, *9*, 438. (c) Ma, S. Q.; Sun, D. F.; Ambrogio, M.; Fillinger, J. A.; Parkin, S.; Zhou, H. C. *J. Am. Chem. Soc.* **2007**, *129*, 1858. (d) Furukawa, H.; Ko, N.; Go, Y. B.; Aratani, N.; Choi, S. B.; Choi, E.; Yazaydin, A. O.; Snurr, R. Q.; O'Keeffe, M.; Kim, J.; Yaghi, O. M. *Science* **2010**, *329*, 424. (e) Yuan, D.; Zhao, D.; Sun, D.; Zhou, H.-C. *Angew. Chem., Int. Ed.* **2010**, *49*, 5357. (f) Wong-Foy, A. G.; Lebel, O.; Matzger, A. J. *J. Am. Chem. Soc.* **2007**, *129*, 15740.

(10) (a) Bae, Y.-S.; Mulfort, K. L.; Frost, H.; Ryan, P.; Punnathanam, S.; Broadbelt, L. J.; Hupp, J. T.; Snurr, R. Q. *Langmuir* **2008**, *24*, 8592. (b) Li, J.-R.; Kuppler, R. J.; Zhou, H.-C. *Chem. Soc. Rev.* **2009**, *38*, 1477. (c) Bae, Y.-S.; Farha, O. K.; Spokoyny, A. M.; Mirkin, C. A.; Hupp, J. T.; Snurr, R. Q. *Chem. Commun.* **2008**, 4135. (d) Banerjee, R.; Furukawa, H.; Britt, D.; Knobler, C.; O'Keeffe, M.; Yaghi, O. M. *J. Am. Chem. Soc.* **2009**, *131*, 3875. (e) Bae, Y.-S.; Farha, O. K.; Hupp, J. T.; Snurr, R. Q. *J. Mater. Chem.* **2009**, *19*, 2131. (f) Blomqvist, A.; Araujo, C. M.; Srepusharawoot, P.; Ahuja, R. *PNAS.* **2007**, *104*, 20173. (g) Li, Z.; Zhu, G.; Lu, G.; Qiu, S.; Yao, X. *J. Am. Chem. Soc.* **2010**, *132*, 1490. (h) Dinca, M.; Dailly, A.; Liu, Y.; Brown, C. M.; Neumann, D. A.; Long, J. R. *J. Am. Chem. Soc.* **2006**, *128*, 16876. (i) Choi, H. J.; Dinca, M.; Dailly, A.; Long, J. R. *Energy Environ. Sci.* **2010**, *3*, 117. (j) Sumida, K.; Horike, S.; Kaye, S. S.; Herm, Z. R.; Queen, W. L.; Brown, C. M.; Grandjean, F.; Long, G. J.; Dailly, A.; Long, J. R. *Chem. Sci.* **2010**, *1*, 184. (k) Dinca, M.; Dailly, A.; Tsay, C.; Long, J. R. *Inorg. Chem.* **2008**, *47*, 11.

(11) (a) Chen, B.; Ockwig, N. W.; Millward, A. R.; Contreras, D. S.; Yaghi, O. M. *Angew. Chem., Int. Ed.* **2005**, *44*, 4745. (b) Chui, S. S.-Y.; Lo, S. M.-F.; Charmant, J. P. H.; Orpen, A. G.; Williams, I. D. *Inorg. Chem. Commun.* **1999**, *283*, 1148. (c) Karra, J. R.; Walton, K. S. *Langmuir* **2008**, *24*, 8620. (d) Schlichte, K.; Kratzke, T.; Kaskel, S. *Microporous Mesoporous Mater.* **2004**, *73*, 81. (e) Prestipino, C.; Regli, L.; Vitillo, J. G.; Bonino, F.; Lamberti, D. C.; Zecchina, A.; Solari, P. L.; Kongshaug, K. O.; Bordiga, S. *Chem. Mater.* **2006**, *18*, 1337. (f) Rosi, N. L.; Kim, J.; Eddaoudi, M.; Chen, B. L.; O'Keeffe, M.; Yaghi, O. M. *J. Am. Chem. Soc.* **2005**, *127*, 1504. (g) Dietzel, P. D. C.; Morita, Y.; Blom, R.; Fjellvag, H. *Angew. Chem., Int. Ed.* **2005**, *44*, 6354. (h) Dietzel, P. D. C.; Panella, B.; Hirscher, M.; Blom, R.; Fjellvag, H. *Chem. Commun.* **2006**, 959. (i) Caskey, S. R.; Wong-Foy, A. G.; Matzger, A. J. *J. Am. Chem. Soc.* **2008**, *130*, 10870.

(12) (a) Chen, Z.; Xiang, S.; Arman, H. D.; Li, P.; Zhao, D.; Chen, B. *Eur. J. Inorg. Chem.* **2011**, 2227. (b) Chen, Z.; Xiang, S.; Arman, H. D.; Li, P.; Tidrow, S.; Zhao, D.; Chen, B. *Eur. J. Inorg. Chem.* **2010**, 3745. (c) Panda, T.; Pachfule, P.; Chen, Y.; Jiang, J.; Banerjee, R. *Chem. Commun.* **2011**, *47*, 2011. (d) Debatin, F.; Thomas, A.; Kelling, A.; Hedin, N.; Bacsik, Z.; Senkovska, I.; Kaskel, S.; Junginger, M.; Muller, H.; Schilde, U.; Jager, C.; Friedrich, A.; Holdt, H.-J. *Angew. Chem., Int. Ed.* **2010**, *49*, 1258. (e) An, J.; Geib, S. J.; Rosi, N. L. *J. Am. Chem. Soc.* **2010**, *132*, 38. (f) Vaidhyanathan, R.; Iremonger, S. S.; Dawson, K. W.; Shimizu, G. K. H. *Chem. Commun.* **2009**, 5230. (g) Arstad, B.; Fjellvag, H.; Kongshaug, K. O.; Swang, O.; Blom, R. *Adsorption* **2008**, *14*, 755. (h) Couck, S.; Denayer, J. F. M.; Baron, G. V.; Remy, T.; Gascon, J.; Kapteijn, F. *J. Am. Chem. Soc.* **2009**, *131*, 6326. (i) Lin, J.-B.; Zhang, J.-P.; Chen, X.-M. *J. Am. Chem. Soc.* **2010**, *132*, 6654. (j) Torrisi, A.; Bell, R. G.; Mellot-Draznieks, C. *Cryst. Growth Des.* **2010**, *10*, 2839. (k) Demessence, A.; D'Alessandro, D. M.; Foo, M. L.; Long, J. R. *J. Am. Chem. Soc.* **2009**, *131*, 8784. (l) Sayari, A.; Belmabkhout, Y. *J. Am. Chem. Soc.* **2010**, *132*, 6312. (m) Gu, X.; Lu, Z.—H.; Xu, Q. *Chem. Commun.* **2010**, *46*, 7400. (n) Yazaydin, A. O.; Snurr, R. Q.; Park, T.-H.; Koh, K.; Liu, J.; LeVan, M. D.; Benin, A. I.; Jakubczak, P.; Lanuza, M.; Galloway, D. B.; Low, J. J.; Willis, R. R. *J. Am. Chem. Soc.* **2009**, *131*, 18198. (o) An, J.; Fiorella, R. P.; Geib, S. J.; Rosi, N. L. *J. Am. Chem. Soc.* **2009**, *131*, 8401.

(13) (a) Yildirim, T.; Hartman, M. R. *Phys. Rev. Lett.* **2005**, *95*, 215504. (b) Hartman, M. R.; Peterson, V. K.; Liu, Y.; Kaye, S. S.; Long, J. R. *Chem. Mater.* **2006**, *18*, 3221. (c) Peterson, V. K.; Liu, Y.; Brown, C. M.; Kepert, C. J. *J. Am. Chem. Soc.* **2007**, *128*, 15578. (d) Wu, H.; Zhou, W.; Yildirim, T. *J. Am. Chem. Soc.* **2007**, *129*, 5314. (e) Rowsell, J. L. C.; Eckert, J.; Yaghi, O. M. *J. Am. Chem. Soc.* **2005**, *127*, 14904. (f) Hubner, O.; Gloss, A.; Fichtner, M.; Klopper, W. *J. Phys. Chem. A* **2004**, *108*, 3019. (g) Liu, Y.; Brown, C. M.; Neumann, D. A.; Peterson, V. K.; Kepert, C. J. *J. Alloys Compd.* **2007**, *446—447*, 385.

(14) (a) Yang, C.; Wang, X.; Omary, M. A. *J. Am. Chem. Soc.* **2007**, *129*, 15454. (b) Yang, C.; Wang, X. P.; Omary, M. A. *Angew. Chem., Int. Ed.* **2009**, *48*, 2500. (c) Fischer, R. A.; Woll, C. *Angew. Chem., Int. Ed.* **2008**, *47*, 8164. (d) Hulvey, Z.; Falcao, E. H. L.; Eckert, J.; Cheetham, A. K. *J. Mater. Chem.* **2009**, *19*, 4307. (e) Hulvey, Z.; Sava, D. A.; Eckert, J.; Cheetham, A. K. *Inorg. Chem.* **2011**, *50*, 403. (f) Pan, L.; Sander, M. B.; Huang, X.; Li, J.; Smith, M.; Bittner, E.; Bockrath, B.; Johnson, J. K. *J. Am. Chem. Soc.* **2004**, *126*, 1308. (g) Yang, W.; Lin, X.; Blake, A. J.; Wilson, C.; Hubberstey, P.; Champness, N. R.; Schroder, M. *Inorg. Chem.* **2009**, *48*, 11067. (h) Fernandez, C. A.; Thallapally, P. K.; Motkuri, R. K.; Nune, S. K.; Sumrak, J. C.; Tian, J.; Liu, J. *Cryst. Growth Des.* **2010**, *10*, 1037.(i) F-MOF-1 data has been independently reviewed by Fischer and Wöll.

(15) Chun, H.; Dybtsev, D. N.; Kim, H.; Kim., K. *Chem.—Eur. J.* **2005**, *11*, 3521.

(16) **Cu-TBA-1**: $C_{86}H_{50}N_{40}O_{22}Cu_9$, M_r = 2567.52, Orthorhombic, *Pnn*2, a = 13.464(8) Å; b = 29.985(17) Å; c = 19.717(11); V = 7960(8) Å^3, D_c = 1.071 g cm^{-3}, μ = 1.235 mm^{-1}, 13908 total reflection, 7177 unique (R_{int} = 0.1456), T = 293(2), final R indices ($I > 2\sigma(I)$): R_1 = 0.0778, wR_2 = 0.1731, Goodness-of-fit = 0.910. **Cu-TBA-2**: $C_{21}H_{23}N_9O_6Cu_2$, M_r = 624.58, Orthorhombic, *Imm*2, a = 7.119(6) Å; b = 21.58(2) Å; c = 9.100(8); V = 1398(2) Å^3, D_c = 1.477 g cm^{-3}, μ = 1.572 mm^{-1}, 1611 total reflection, 1459 unique (R_{int} = 0.0701), T = 293(2), final R indices ($I > 2\sigma(I)$): R_1 = 0.0604, wR_2 = 0.1503, Goodness-of-fit = 1.077. **Cu-TBA-2F**: $C_{11.16}H_8F_{0.33}N_5O_3Cu$, M_r = 330.09, Orthorhombic, *Ima*2, a = 7.1850(15) Å; b = 9.1854(19) Å; c = 21.544(5); V = 1421.8(5) Å^3, D_c = 1.540 g cm^{-3}, μ = 1.553 mm^{-1}, 1799 total reflection, 1335 unique (R_{int} = 0.0694), T = 293(2), final R indices ($I > 2\sigma(I)$): R_1 = 0.0723, wR_2 = 0.1961, Goodness-of-fit = 1.031. CCDC 811812—811814.

(17) Here it should be noted that Fluorinated Metal Organic Framework (*F*-MOF) referred here is not fully fluorinated, but it is the partially fluorinated where only one hydrogen atom from 2 position of 4-TBA is replaced by fluorine. (a) Song, W.-C.; Li, J.-R.; Song, P.-C.; Tao, Y.; Yu, Q.; Tong, X.-L.; Bu, X.-H. *Inorg. Chem.* **2009**, *48*, 3792. (b) Ouellette, W.; Liu, H.; Whitenack, K.; O'Connor, C. J.; Zubieta, J. *Cryst. Growth Des.* **2009**, *9*, 4258. (c) Jiang, T.; Zhao, Y.-F.; Zhang, X.-M. *Inorg. Chem. Commun.* **2007**, *10*, 1194. (d) Li, Y.; Xu, G.; Zou, W,-Q.; Wang, M.-S.; Zheng, F.-K.; Wu, M.-F.; Zeng, H.-Y.; Guo, G.-C.; Huang, J.-S. *Inorg. Chem.* **2008**, *47*, 7945. (e) Guo, H.; Guo, X.; Wang, X.; Li, G.; Guo, Z.; Su, S.; Zhang, H. *CrystEngComm.* **2009**, *11*, 1509.

(18) Koyama, M.; Ohtani, N.; Kai, F.; Moriguchi, I.; Inouye, S. *J. Med. Chem.* **1987**, *30*, 552.

(19) *SMART*, Version 5.05; Bruker AXS, Inc.: Madison, WI, 1998.

(20) *SAINT-Plus*, Version 7.03; Bruker AXS Inc.: Madison, WI, 2004.

(21) Sheldrick, G. M. *SADABS*, Version 2.03, and *TWINABS*, Version 1.02; University of Göttingen: Göttingen, Germany, 2002.

(22) Sheldrick, G. M. *SHELXS-97*; University of Göttingen: Göttingen, Germany, 1997.

(23) Sheldrick, G. M. *SHELXTL-97*;University of Göttingen: Göttingen, Germany, 1997.
(24) Spek, A. L. *PLATON, A Multipurpose Crystallographic Tool*; Utrecht University: Utrecht, The Netherlands, 2005.
(25) *Materials Studio*; Accelrys: San Diego, CA, 2007.
(26) Cracknell, R. F. *Phys. Chem. Chem. Phys.* **2001**, *3*, 2091.
(27) Rappe, A. K.; Casewit, C. J.; Colwell, K. S.; Goddard, W. A.; Skiff, W. M. *J. Am. Chem. Soc.* **1992**, *114*, 10024.
(28) The experimental pattern of Cu-TBA-1 has a few diffraction lines that are unindexed and some that are slightly broadened in comparison with those simulated patterns. This is probably due to the loss of either DMF or EtOH molecules from the lattice or phase change due to grinding while at analysis.
(29) (a) Zhao, X.; Xiao, B.; Fletcher, A. J.; Thomas, K. M.; Bradshaw, D.; Rosseinsky, M. J. *Science* **2004**, *306*, 1012. (b) Panella, B.; Hirscher, M. *Adv. Mater.* **2005**, *17*, 538.(c) Breck, D. W. *Zeolite molecular sieves*; John Wiley and Sons: New York, 1974. (d) Wegrzyn, J.; Gurevich, M. *Appl. Energy.* **1996**, *55*, 71. (e) Ma, S.; Sun, D.; Simmons, J. M.; Collier, C. D.; Yuan, D.; Zhou, H.-C. *J. Am. Chem. Soc.* **2008**, *130*, 1012. (f) Rowsell, J. L. C.; Yaghi, O. M. *Angew. Chem., Int. Ed.* **2005**, *44*, 4670. (g) Collins, D. J.; Zhou, H.-C. *J. Mater. Chem.* **2007**, *17*, 3154. (h) Sun, D.; Ma, S.; Ke, Y.; Collins, D. J.; Zhou, H.-C. *J. Am. Chem. Soc.* **2006**, *128*, 3896. (i) Kondo, M.; Shimamura, M.; Noro, S.-I.; Minakoshi, S.; Asami, A.; Seki, K.; Kitagawa, S. *Chem. Mater.* **2000**, *12*, 1288. (j) Bourrelly, S.; Llewellyn, P. L.; Serre, C.; Millange, F.; Loiseau, T.; Ferey, G. *J. Am. Chem. Soc.* **2005**, *127*, 13519. (k) Dueren, T.; Sarkisov, L.; Yaghi, O. M.; Snurr, R. Q. *Langmuir* **2004**, *20*, 2683.
(30) (a) Park, K. S.; Ni, Z.; Cote, A. P.; Choi, J. Y.; Huang, R. D.; Uribe-Romo, F. J.; Chae, H. K.; O'Keeffe, M.; Yaghi, O. M. *Proc. Natl. Acad. Sci. U. S. A* **2006**, *103*, 10186. (b) Zhou, W.; Wu, H.; Hartman, M. R.; Yildirim, T. *J. Phys. Chem. C* **2007**, *111*, 16131. (c) Chen, B. L.; Ma, S. Q.; Hurtado, E. J.; Lobkovsky, E. B.; Zhou, H. C. *Inorg. Chem.* **2007**, *46*, 8490. (d) Chen, B. L.; Liang, C. D.; Yang, J.; Contreras, D. S.; Clancy, Y. L.; Lobkovsky, E. B.; Yaghi, O. M.; Dai, S. *Angew. Chem., Int. Ed.* **2006**, *45*, 1390. (e) Wong-Foy, A. G.; Matzger, A. J.; Yaghi, O. M. *J. Am. Chem. Soc.* **2006**, *128*, 3494. (f) Rowsell, J. L. C.; Yaghi, O. M. *J. Am. Chem. Soc.* **2006**, *128*, 1304. (g) Dailly, A.; Vajo, J. J.; Ahn, C. C. *J. Phys. Chem. B* **2006**, *110*, 1099. (h) Zhao, D.; Yuan, D.; Zhou, H.-C. *Energy Environ. Sci.* **2008**, *1*, 222.
(31) We replaced the 2-F-4-TBA with 3-F-4-TBA, which is the 3-substituted fluorinated analogue of 4-TBA. The reaction of 3-F-4-TBA with $Cu(NO_3)_2$ was resulted into the formation of plate like blue crystals similar to Cu-TBA-2 and Cu-TBA-2F. But in this case, we are unable to grow proper sized crystals for single crystal X-ray diffraction studies after several attempts. The formation of same phase like Cu-TBA-2 and Cu-TBA-2F was confirmed by PXRD studies in the case of Cu-TBA-3F (see Supporting Information, Figure S4).